

Implicit Grid Convolution for Multi-Scale Image Super-Resolution

Dongheon Lee, Seokju Yun, Youngmin Ro*

University of Seoul

{dslisleedh, wsz871, youngmin.ro}@uos.ac.kr

code: <https://github.com/dslisleedh/IGConv>

Abstract

Recently, Super-Resolution (SR) achieved significant performance improvement by employing neural networks. Most SR methods conventionally train a single model for each targeted scale, which increases redundancy in training and deployment in proportion to the number of scales targeted. This paper challenges this conventional fixed-scale approach. Our preliminary analysis reveals that, surprisingly, encoders trained at different scales extract similar features from images. Furthermore, the commonly used scale-specific upsampler, Sub-Pixel Convolution (SPConv), exhibits significant inter-scale correlations. Based on these observations, we propose a framework for training multiple integer scales simultaneously with a single model. We use a single encoder to extract features and introduce a novel upsampler, Implicit Grid Convolution (IGConv), which integrates SPConv at all scales within a single module to predict multiple scales. Our extensive experiments demonstrate that training multiple scales with a single model reduces the training budget and stored parameters by one-third while achieving equivalent inference latency and comparable performance. Furthermore, we propose IGConv⁺, which addresses spectral bias and input-independent upsampling and uses ensemble prediction to improve performance. As a result, SRFormer-IGConv⁺ achieves a remarkable 0.25dB improvement in PSNR at Urban100×4 while reducing the training budget, stored parameters, and inference cost compared to the existing SRFormer.

1 Introduction

Super-Resolution (SR) aims to restore a High-Resolution Image (I^{HR}) from a Low-Resolution Image (I^{LR}) input, which is one of the most fundamental challenges in computer vision and graphics. Over a decade ago, SRCNN (Dong et al. 2015) successfully introduced neural networks to SR, leading to significant performance improvements. Following SRCNN, many previous studies have focused on improving performance by proposing new core operators or larger models, leading to models like ATD (Zhang et al. 2024) that use as many as 20 million parameters.

Conventionally, many SR studies take the fixed-scale training approach, where a single scale-specific model is trained for each scale, for granted. This approach significantly increases the training budget and stored parameters,

*Corresponding Author

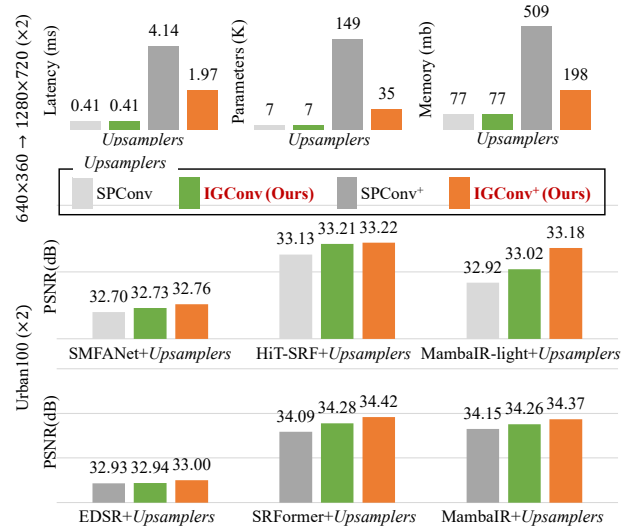


Figure 1: Efficiency and performance comparison on existing upsampler (SPConv and SPConv+) with our proposals (IGConv and IGConv+) on various metrics and models. Efficiency metrics are measured by reconstructing an HD (1280×720) image on an A6000 GPU after instantiating our proposals on a ×2 scale.

making finding the optimal hyper-parameters more challenging and requiring additional research effort. For instance, since SR typically considers three scales (×2, ×3, and ×4), the MambaR (Guo et al. 2024), which takes 241 hours to train using four A6000 GPUs, should spend a total of 723 hours to train. In addition, the necessity of storing and utilizing models for all target scales makes deployment challenging, particularly in situations with limited computational resources.

This paper challenges the conventional fixed-scale approach and conducts preliminary analysis. Surprisingly, we find that models trained on different scales extract similar features. Additionally, we discover that the commonly used scale-specific upsampler, Sub-Pixel Convolution (SPConv), exhibits significant inter-scale correlation in its functionality. Based on these observations, we aim to integrate multiple-scale models into a single model. This is closely re-

lated to the methods in the Arbitrary-Scale Super-Resolution (ASSR) domain; however, ASSR methods consume excessive computation due to their inefficient architecture for predicting non-integer scales. As shown in Table 1, LM-LTE (He and Jin 2024) exhibits $25\times$ higher latency than our method, yet achieves a PSNR of 0.19 dB lower on Urban100 $\times 4$. To this end, we propose a multi-scale framework that allows training multiple integer scales with a single model. We design a model that uses a single encoder to extract features across all scales and introduce a novel upsampler Implicit Grid Convolution (IGConv), which integrates SPConv across all scales into a unified module. Our extensive experiments demonstrate that multi-scale training with IGConv **reduces the training budget and stored parameters by one-third while maintaining or improving performance** compared to models trained on a fixed scale.

In addition, we propose IGConv⁺, which boosts performance by addressing spectral bias, input-independent upsampling, and ensembled prediction. We use frequency loss to mitigate spectral bias and introduce a computationally efficient upsampling method called Implicit Grid Sampling (IGSample) to address input-independent upsampling. Additionally, we introduce a feature-level geometric reparameterization (FGRep) that enables ensembled prediction with a single forward pass. Our thorough experiments validate that IGConv⁺, when applied to EDSR, SRFormer, and MambaIR proposed for fixed-scale training, **improves PSNR by 0.16dB, 0.25dB, and 0.12dB, respectively, on Urban100 $\times 4$, with reduced training budgets, stored parameters, and inference costs.**

Our contributions are summarized as follows:

- We highlight the redundancy of classic fixed-scale SR methods and address this by proposing a multi-scale training framework introducing IGConv.
- Furthermore, we propose IGConv⁺, which improves performance by employing frequency loss, introducing IGSample, and FGRep
- As a result, SRFormer-IGConv⁺ trained on multiple scales achieves a remarkable 0.33dB improvement in PSNR on Urban100 $\times 2$.

Table 1: Comparison of various upsamplers. The efficiency metrics are measured by upsampling a 256×256 image for scale $\times 4$ using an A6000 GPU.

Upsampler (@RDN)	Type	Latency (ms)	Memory (mb)	Urban100		
				$\times 2$	$\times 3$	$\times 4$
SPConv ⁺	Fixed.	5.5	529.1	32.89	28.80	26.61
LM-LTE (CVPR'24)	Arb.	95.7	1442.4	33.03	28.96	26.80
IGConv⁺ (Ours)	Multi.	3.9	193.5	33.17	29.11	26.96

2 Related Work

2.1 Classic Super-Resolution

From early on to the present, CNN-based models, which primarily utilize convolution operations suited for image processing due to their local bias and translation invariance, have been foundational in SR tasks (Dong et al. 2015; Shi

et al. 2016; Lim et al. 2017; Zhang et al. 2018a; Zheng et al. 2024). Recently, transformers (Vaswani et al. 2017) have garnered significant attention in SR tasks due to their ability to effectively handle long-range dependencies and their advantage of using dynamic weights. However, the original self-attention computation has a complexity that scales quadratically with the number of pixels, making it unsuitable for low-level vision tasks that deal with large images. To address this issue, approaches that reduce complexity by computing self-attention within a window patch (Liang et al. 2021) or in a transposed manner (channel-wise) (Zamir et al. 2022) have been successfully introduced to low-level vision tasks with superior performance with lower computational complexity and parameters. Building on the success of window/transposed self-attention, studies have continued to report improvements in various aspects: widening receptive fields of transformers (Chen et al. 2023b; Zhou et al. 2023; Zhang, Zhang, and Yu 2024; Ray, Kumar, and Kolekar 2024; Zhang et al. 2024), spectral bias (Li et al. 2023), and overall efficiency (Zhang et al. 2022; Liu et al. 2023b). Despite the advancements, window/transposed self-attention still faces the inherent limitation of quadratic complexity in the number of pixels computed. As a promising alternative, MambaIR (Guo et al. 2024), successfully applied to low-level vision tasks by improving the local and channel processing power of state-space models with complexity growing linearly with the number of pixels computed, has gained renewed attention.

Most listed studies adopt SPConv for upsampling and employ a single model for a single scale. In contrast, we utilize various methods to propose a multi-scale training framework that allows a single model to train multiple integer scales.

2.2 Multi/Arbitrary-Scale Super-Resolution

Unlike the class SR methods, there have been experimental attempts to train more than one scale with a single model. For example, LapSRN (Lai et al. 2017) proposed an architecture that progressively upsamples image to predict $\times 8$ scale reliably, MDSR (Lim et al. 2017) shared a feature extractor across all scales and used scale-specific heads and tails, and MetaSR (Hu et al. 2019) proposed a meta-upscaling module that parameterizes the convolution filters by relative position and scale for ASSR. Recently, research in the ASSR field has gained significant attention by adopting Implicit Neural Representation (INR) from the graphics domain (Wang et al. 2021). LIIF uses the deep feature representation extracted by the encoder from I_{LR} along with 2-D coordinates to predict RGBs at corresponding locations using an MLP, thereby learning an implicit continuous representation of the image. Subsequent studies have focused on improving aspects such as the spectral bias (Lee and Jin 2022), local ensemble (Cao et al. 2023; Chen et al. 2023a), scale-equivalence (Wang et al. 2023), and efficiency (Song et al. 2023; He and Jin 2024; Vasconcelos et al. 2023).

While our approach is similar to ASSR methods in that we aim to train multiple scales with a single model using INR-based methods, we differ in that we do not target arbitrary scales. Furthermore, we demonstrate that our methodology is superior to existing multi-scale methods in Appendix A.

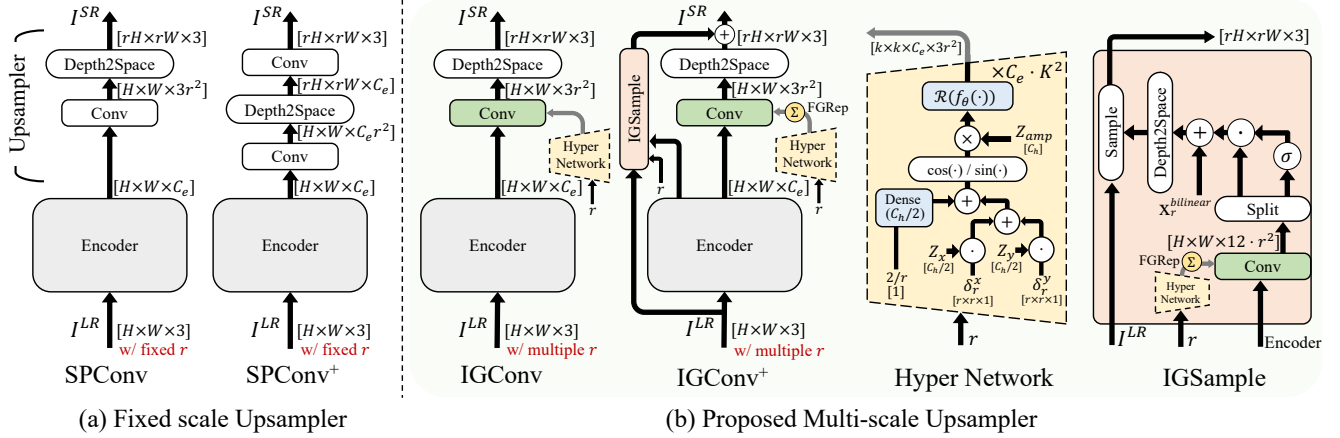


Figure 2: The structure of SR models. (a) illustrates the architectures employing a fixed-scale upsampler, while (b) illustrates the architecture employing our proposed multi-scale upsampler. Our proposed methods comprise the hyper-network to generate a convolution kernel based on scale and employ the IGSample as a sub-module to perform input-dependent upsampling efficiently. FGRep is employed to improve performance by performing ensemble prediction without additional computation.

3 Proposed Methods

This section explains the structure of existing SR models and presents the preliminary analyses that led to our proposal to train multiple integer scales with a single model. Based on the above analyses, we introduce our novel upsampler, IGConv, capable of predicting multiple integer scales efficiently. Following that, we describe the methods added to IGConv+ – frequency loss, IGSample, and FGRep – to enhance performance further.

3.1 Structure of SR Models

As shown in Figure 2, the structure of SR Models consists of an encoder and an upsampler, and it can be presented as:

$$\begin{aligned} M &= \mathcal{E}(I^{LR}), \\ I^{SR} &= \mathcal{U}(M, r), \end{aligned} \quad (1)$$

where \mathcal{E} denotes the encoder that extracts deep feature representation $M \in \mathbb{R}^{H \times W \times C_e}$ with the same resolution as the input $I^{LR} \in \mathbb{R}^{H \times W \times 3}$, and \mathcal{U} represents the upsampler that produces target output $I^{SR} \in \mathbb{R}^{rH \times rW \times 3}$ with scale factor r . Note that the SR methods train a single model on a specific scale, requiring separate encoders and upsamplers for each scale. In contrast, we train multiple integer scales with a single model, utilizing a single pair of encoder and decoder.

3.2 Preliminary Analysis

Many SR studies train and evaluate separate models for each scale (Lim et al. 2017; Zhou et al. 2023; Zheng et al. 2024; Zhang, Zhang, and Yu 2024; Guo et al. 2024), treating each scale as a different degradation problem. As shown in Figure 3, however, we find that even though the model was trained on different scales, the CKA similarity of the encoder’s final output exceeds 90% on average. This result

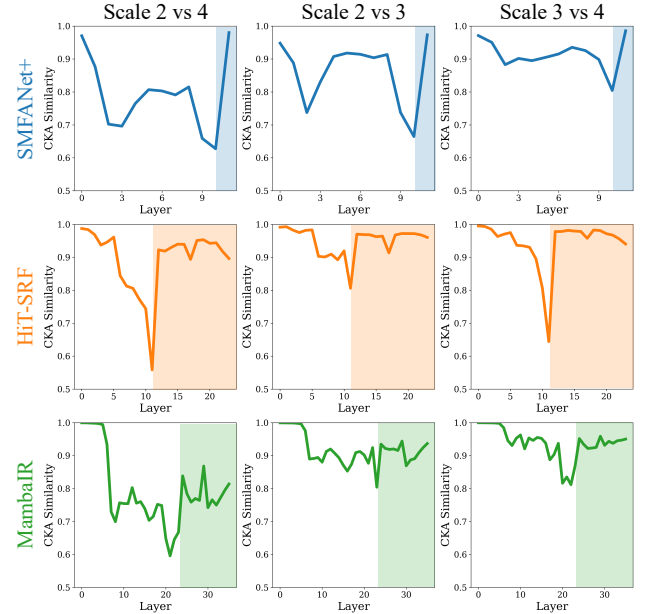


Figure 3: Visualization of CKA similarity between feature maps at scale $\times 2$, $\times 3$, and $\times 4$ varying layers of SMFANet+, HiT-SRF, and MambaIR. CKA similarity demonstrates that feature maps at different scales become increasingly similar as they approach the later layer.

suggests that encoders at different scales extract similar features, indicating the potential for a single encoder to learn across various scales. In addition, we investigate the mechanism of SPConv (decoder), where each convolution filter that produces different scales can be highly correlated, as shown in Figure 4. For instance, the number of filters that predict $r = 4$ and $r = 2$ are different, 4^2 and 2^2 , respec-

tively, but the areas they predict are highly correlated. Our analysis confirms that the upsampler’s input, M , remains largely unchanged across different r values, suggesting that a scale-specific encoder is unnecessary. It also demonstrates that the existing SPConv modules across all scales can be unified into a single module due to their strong inter-scale correlations.

3.3 Implicit Grid Convolution

We propose IGConv, which integrates SPConv across all scales by parameterizing its convolution filters with inter-scale correlations – specifically, the relative coordinates and sizes of sub-pixels in the predicted area that vary with r – employing a hyper-network. IGConv consists of three main components: the hyper-network, convolution operation, and upsampling operation. These can be represented as follows:

$$\begin{aligned} K &= \mathcal{H}(r), \\ M' &= M * K, \\ I^{SR} &= \mathcal{DS}(M', r), \end{aligned} \quad (2)$$

where \mathcal{H} represents the hyper-network that generates the convolution filter K ($\in \mathbb{R}^{k \times k \times C_e \times 3 \cdot r^2}$) according to r , and M' ($\in \mathbb{R}^{H \times W \times 3 \cdot r^2}$) refers to the feature map obtained by convolving M with K . M' is then passed through the upsampling operation \mathcal{DS} ($: \mathbb{R}^{H \times W \times 3 \cdot r^2} \rightarrow \mathbb{R}^{rH \times rW \times 3}$), resulting in I_{SR} .

Since \mathcal{H} depends only on r , it can be pre-computed and eliminated by instantiating IGConv at a specific r during inference, making the instantiated IGConv functionally identical to SPConv. Furthermore, because IGConv does not introduce additional modules to the encoder, the model with instantiated IGConv maintains the same computational cost as the model with SPConv.

HyperNetwork The hyper-network aims to generate K according to the given r , and it is formulated as follows:

$$\begin{aligned} F_r &= h(r), \\ K' &= f_\theta(F_r), \\ K &= \mathcal{R}(K'), \end{aligned} \quad (3)$$

where h represents the coefficient estimator that generates Fourier coefficients F_r ($\in \mathbb{R}^{C_e \cdot k^2 \times r \times r \times C_h}$) according to the r , and f_θ is parameterized MLPs with ReLU activations that predict the intermediate convolution kernel K' ($\in \mathbb{R}^{C_e \cdot k^2 \times r \times r \times 3}$) from the Fourier coefficients. Lastly, \mathcal{R} denotes the reshape operation that converts the K' into K for a suitable data structure for convolution. Specifically, F_r is inferred through the following process:

$$\begin{aligned} C_r &= \delta_r^x \odot Z^x + \delta_r^y \odot Z^y, s_r = h^s(2/r), \\ F_r &= Z_{amp} \odot \begin{bmatrix} \cos(\pi(C_r + s_r)) \\ \sin(\pi(C_r + s_r)) \end{bmatrix}, \end{aligned} \quad (4)$$

where Z_{amp} ($\in \mathbb{R}^{C_h}$) denotes the scale-invariant latent code, C_r ($\in \mathbb{R}^{C_e \cdot k^2 \times r \times r \times C_h}$) refers to the coordinate matrix representing the relative coordinates according to the r , and s_r represents the size according to the

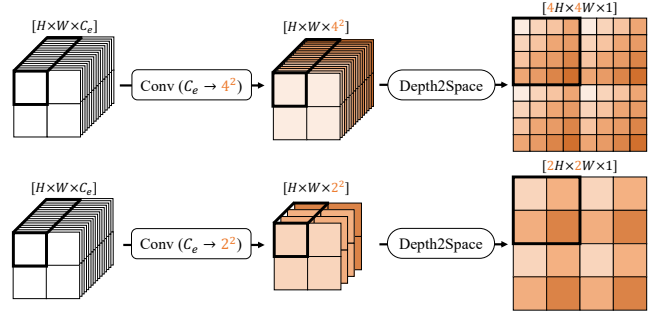


Figure 4: Visualization of SPConv for scales 2 and 4. Although the SPConvs at different scales employ different numbers of filters, the filtered outputs for all scales exhibit significant 2D spatial correlations (illustrated with color gradients) due to the subsequent depth-to-space operation. Visualized kernels that are trained to capture inter-scale correlations are shown in Figure 5.

r . F_r is created by element-wise multiplying the scale-dependent Fourier matrix, formed by C_r and s_r , with Z_{amp} . C_r is generated by element-wise multiplying the uniformly sampled 2D relative coordinates δ_r^x, δ_r^y ($\in [-1, 1]^{1 \times r \times r \times 1}$) with the coordinate-invariant latent codes Z^x, Z^y ($\in \mathbb{R}^{C_e \cdot k^2 \times 1 \times 1 \times C_h/2}$) respectively, and then summing the results. s_r is generated by feeding the reciprocal of the r , proportional to the size, into a single linear layer (h^s).

3.4 Frequency Loss

Mapping signals using an MLP induces spectral bias (Lee and Jin 2022). Therefore, in addition to the commonly used pixel-wise L1 loss, we use a frequency loss (Tu et al. 2022; Sun, Pan, and Tang 2022) to make the model focus on high-frequency detail, as follows:

$$\mathcal{L} = \|I^{HR} - I^{SR}\|_1 + \lambda \|\mathcal{F}(I^{HR}) - \mathcal{F}(I^{SR})\|_1, \quad (5)$$

where \mathcal{F} denotes the Fast Fourier transform, and λ is a weight parameter set to be 0.05 empirically.

3.5 IGSample Residual Skip

SPConv has a limitation in performance, upscaling the input M without leveraging the input information. For this reason, many SR studies that focus on performance improvements use SPConv⁺, which adds a convolution after \mathcal{DS} (see Figure 2). However, SPConv⁺ has a nearly 10 \times latency increase over SPConv because the additional convolution is performed in upsampled high-resolution (HR) space. To address this, inspired by previous research aimed at upsampling feature maps (Liu et al. 2023a), we propose IGSample, as formulated below:

$$\begin{aligned} K^o, K^s &= \mathcal{H}_S(r), \\ \delta^{xy} &= (M * K^o) \odot \sigma(M * K^s), \\ x_r &= \mathcal{DS}(x_r^{bilinear} + \delta^{xy}, r), \\ I^S &= \mathcal{S}(I^{LR}, \text{coord}), \end{aligned} \quad (6)$$

Table 2: Comparisons of fixed-scale upsamplers (SPConv, SPConv⁺) and our proposed multi-scale upsamplers (IGConv, IGConv⁺) on various encoders trained on the DIV2K dataset. The only best results are bolded.

Dataset	Scale	Encoder (Operator)	Upsampler	Set5	Set14	B100	Urban100	Manga109
DIV2K	2	EDSR (CNN)	SPConv ⁺	38.11/0.9602	33.92/0.9195	32.32/0.9013	32.93/0.9351	39.10/0.9773
			IGConv	38.21/0.9612	33.96/0.9209	32.34/0.9016	32.94/0.9359	39.13/0.9780
			IGConv ⁺	38.24/0.9614	33.96/0.9209	32.34/ 0.9018	33.00/0.9360	39.25/0.9783
		HiT-SRF (Transformer)	SPConv	38.26/0.9615	34.01/0.9214	32.37/0.9023	33.13/0.9372	39.47/ 0.9787
			IGConv	38.16/0.9604	34.02/0.9214	32.35/0.9020	33.21/0.9377	39.34/0.9781
			IGConv ⁺	38.30/0.9615	33.97/0.9210	32.38/0.9023	33.22/0.9377	39.47/0.9786
		MambaIR-light (SSM)	SPConv	38.16/0.9610	34.00/0.9212	32.34/0.9017	32.92/0.9356	39.31/0.9779
			IGConv	38.20/0.9611	34.02/0.9214	32.34/0.9014	33.02/0.9365	39.28/0.9782
			IGConv ⁺	38.20/0.9613	34.11/0.9221	32.36/0.9019	33.18/0.9372	39.44/0.9786
	3	EDSR (CNN)	SPConv ⁺	34.65/0.9280	30.52/0.8462	29.25/0.8093	28.80/0.8653	34.17/0.9476
			IGConv	34.70/0.9294	30.56/0.8469	29.28/0.8097	28.90/0.8671	34.31/0.9491
			IGConv ⁺	34.74/0.9298	30.65/0.8481	29.30/0.8103	28.95/0.8675	34.47/0.9496
		HiT-SRF (Transformer)	SPConv	34.75/0.9300	30.61/0.8475	29.29/0.8106	28.99/0.8687	34.53/0.9502
			IGConv	34.69/0.9292	30.60/0.8476	29.26/0.8098	29.02/ 0.8694	34.46/0.9499
			IGConv ⁺	34.78/0.9302	30.69/0.8488	29.32/0.8111	29.06/0.8693	34.67/0.9506
		MambaIR-light (SSM)	SPConv	34.72/0.9296	30.63/0.8475	29.29/0.8099	29.00/ 0.8689	34.39/0.9495
			IGConv	34.70/0.9294	30.59/0.8474	29.27/0.8094	28.91/0.8672	34.37/0.9492
			IGConv ⁺	34.74/0.9298	30.68/0.8487	29.30/0.8105	29.04/0.8687	34.62/0.9502
	4	EDSR (CNN)	SPConv ⁺	32.46/0.8968	28.80/0.7876	27.71/0.7420	26.64/0.8033	31.02/0.9148
			IGConv	32.57/0.8990	28.84/0.7880	27.76/0.7426	26.75/0.8060	31.29/0.9178
			IGConv ⁺	32.59/0.8996	28.91/0.7890	27.79/0.7433	26.82/0.8064	31.43/0.9182
		HiT-SRF (Transformer)	SPConv	32.55/0.8999	28.87/0.7880	27.75/0.7432	26.80/0.8069	31.26/0.9171
			IGConv	32.53/0.8988	28.90/0.7887	27.71/0.7422	26.88/ 0.8085	31.31/0.9184
			IGConv ⁺	32.60/0.9001	28.95/0.7892	27.80/0.7440	26.91/0.8083	31.57/0.9198
MambaIR-light (SSM)		SPConv	32.51/0.8993	28.85/0.7876	27.75/0.7423	26.75/0.8051	31.26/0.9175	
		IGConv	32.50/0.8992	28.86/0.7879	27.75/0.7422	26.72/0.8045	31.29/0.9175	
		IGConv ⁺	32.62/0.8997	28.93/0.7893	27.80/0.7437	26.87/0.8068	31.51/0.9185	

where \mathcal{H}_S denotes hyper-network to predict convolution filters (K^o , K^s) depending on r same as \mathcal{H} in IGConv. K^o and K^s predict the direction and constraint scope by performing convolution with M . After applying a sigmoid (σ) to the predicted scope, it is multiplied element-wise with the direction to generate δ^{xy} for calibrating the coordinates. Subsequently, δ^{xy} is added to the bilinear sampling coordinate ($x_r^{bilinear}$) according to the scale and then transformed into a suitable data structure for sampling through the \mathcal{DS} operation to create the calibrated sampling coordinate (x_r). Finally, the upsampled image I^S is created by sampling (\mathcal{S}) from I_{LR} based on x_r and then added to I^{SR} . As a result, the IGSample upsamples I^{LR} input-dependently by adjusting the bilinear upsampling coordinates utilizing information from M while shifting the decoder’s role from inferring RGB values to inferring the residual image, thereby allowing it to focus on high-frequency details (Lee and Jin 2022).

3.6 Feature-level Geometric Re-param.

We propose FGRep inspired by input-level geometric ensemble (Lim et al. 2017) and feature-level local ensemble (Chen, Liu, and Wang 2021) to improve performance by leveraging ensemble prediction, defined as follows:

$$M' = \frac{1}{8} \sum_{i=1}^8 \text{Aug}_i^{-1}(\text{Aug}_i(M) * K), \quad (7)$$

where Aug refers to an augmentation function that consists of 8 transformations, including flip, rotation, and identity. FGRep performs each Aug on M to create augmented versions of M , followed by convolution with K . Then, Aug^{-1}

is applied to each filtered output to revert them to their original state, and all filtered outputs are averaged to produce M' . The \mathcal{H} , and \mathcal{DS} in IGConv are omitted.

This is similar to the local ensemble as it performs the ensemble at the feature level but resembles the geometric ensemble in how augmentation is performed. Interestingly, performing convolution on augmented feature maps with a single kernel followed by inverse augmentation is equivalent to applying convolution to a single feature map with augmented kernels, leading to the redefinition of Equation 7 as follows:

$$M' = \frac{1}{8} \sum_{i=1}^8 M * \text{Aug}_i(K). \quad (8)$$

Furthermore, performing convolution on a single feature map with multiple kernels can be converted to performing convolution on a single feature map with a single kernel via structural re-parameterization. Equation 8 is redefined by structural re-parameterization as:

$$M' = M * \bar{K}, \quad (9)$$

$$\text{where } \bar{K} = \frac{1}{8} \sum_{i=1}^8 \text{Aug}_i(K). \quad (10)$$

Consequently, FGRep allows IGConv to generate ensemble predictions without increasing the computational cost during inference. We apply FGRep to every kernel predicted by the hyper-networks (K , K^o , K^s).

Table 3: Comparisons of fixed-scale upsamplers (SPConv, SPConv⁺) and our proposed multi-scale upsamplers (IGConv, IGConv⁺) on various encoders trained on the DF2K dataset. The only best results are bolded.

Dataset	Scale	Encoder (Operator)	Upsampler	Set5	Set14	B100	Urban100	Manga109
DF2K	2	SMFANet+ (CNN)	SPConv	38.19 /0.9611	33.92/0.9207	32.32/ 0.9015	32.70/0.9331	39.46 / 0.9787
			IGConv	38.16/0.9610	33.96 / 0.9213	32.32/0.9014	32.73/0.9332	39.38/0.9785
			IGConv ⁺	38.14/0.9611	33.92/0.9208	32.32/0.9014	32.76 / 0.9334	39.40/0.9786
		SRFormer (Transformer)	SPConv ⁺	38.51/ 0.9627	34.44/0.9253	32.57/0.9046	34.09/0.9449	40.07 / 0.9802
			IGConv	38.44/0.9625	34.64/0.9267	32.56/0.9048	34.28/0.9462	39.88/0.9798
			IGConv ⁺	38.53 /0.9626	34.72 / 0.9268	32.60 / 0.9052	34.42 / 0.9468	40.03/0.9797
		MambaIR (SSM)	SPConv ⁺	38.57 / 0.9627	34.67/0.9261	32.58/0.9048	34.15/0.9446	40.28 / 0.9806
			IGConv	38.48/0.9624	34.68/0.9264	32.58/0.9047	34.26/0.9453	40.14/0.9803
			IGConv ⁺	38.55/0.9625	34.81 / 0.9270	32.62 / 0.9052	34.37 / 0.9461	40.19/0.9802
	3	SMFANet+ (CNN)	SPConv	34.66 / 0.9292	30.57/0.8461	29.25/0.8090	28.67 / 0.8611	34.45/0.9490
			IGConv	34.62/0.9290	30.56/0.8461	29.25/0.8090	28.64/0.8606	34.45/0.9490
			IGConv ⁺	34.58/0.9287	30.58 / 0.8464	29.24/0.8089	28.66/0.8610	34.45/0.9490
		SRFormer (Transformer)	SPConv ⁺	35.02/0.9323	30.94/0.8540	29.48/0.8156	30.04/0.8865	35.26/0.9543
			IGConv	34.96/0.9323	30.95/0.8543	29.47/0.8157	30.11/0.8876	35.16/0.9543
			IGConv ⁺	35.08 / 0.9329	31.06 / 0.8551	29.52 / 0.8166	30.25 / 0.8888	35.45 / 0.9550
		MambaIR (SSM)	SPConv ⁺	35.08/0.9323	30.99/0.8536	29.51/0.8157	29.93/0.8841	35.43/0.9546
			IGConv	35.04/0.9320	31.01/0.8535	29.50/0.8154	29.95/0.8844	35.44/0.9545
			IGConv ⁺	35.10 / 0.9325	31.14 / 0.8550	29.55 / 0.8164	30.11 / 0.8864	35.55 / 0.9549
	4	SMFANet+ (CNN)	SPConv	32.51/0.8985	28.87 / 0.7872	27.74/0.7412	26.56 / 0.7976	31.29/ 0.9163
			IGConv	32.47/0.8982	28.84/0.7866	27.74/0.7413	26.54/0.7969	31.28/0.9158
			IGConv ⁺	32.52 / 0.8988	28.83/0.7867	27.74/0.7413	26.55/0.7974	31.29/0.9161
		SRFormer (Transformer)	SPConv ⁺	32.93/0.9041	29.08/0.7953	27.94/0.7502	27.68/0.8311	32.21/0.9271
			IGConv	32.87/0.9046	29.08/0.7952	27.91/0.7499	27.79/0.8333	32.14/0.9274
			IGConv ⁺	33.04 / 0.9047	29.22 / 0.7971	27.99 / 0.7509	27.93 / 0.8350	32.45 / 0.9288
MambaIR (SSM)		SPConv ⁺	33.03/ 0.9046	29.20/0.7961	27.98/0.7503	27.68/0.8287	32.32/0.9272	
		IGConv	32.98/0.9041	29.17/0.7955	27.97/0.7498	27.68/0.8288	32.36/0.9271	
		IGConv ⁺	33.05 /0.9045	29.25 / 0.7969	28.02 / 0.7512	27.80 / 0.8314	32.52 / 0.9280	

4 Experiments

4.1 Training Pipeline

This section describes the training pipeline to train multiple integer scales simultaneously. We randomly sample a scale from $r \in \{2, 3, 4\}$ for each batch, commonly used in SR tasks. After that, we crop a patch (I_{HR}) from a high-quality image (I_{GT}) to the size of the training patch multiplied by the sampled r . I_{HR} is then bicubic downsampled by the randomly sampled r to create I_{LR} , and model is trained to reconstruct I_{HR} from I_{LR} . Since IGConv can only upsample a single scale per batch, we optimize the model by utilizing generalized gradients averaged across multiple batches. Learning with multiple batches can be achieved through gradient accumulation or distributed learning, and we use distributed learning with 4 GPUs. **In all cases, we train all scales ($\times 2$, $\times 3$, and $\times 4$) simultaneously, but only with the training budget that existing fixed-scale methods used for the $\times 2$ scale.**

4.2 Implementation details

In this section, we describe the implementation details of our proposal methods. The f_θ of \mathcal{H} and \mathcal{H}_S are composed of 256 and 128 dimensions, respectively, with four and two hidden layers. Additionally, C_h for both \mathcal{H} and \mathcal{H}_S are also set to 256 and 128, respectively. Following the previous study (Lee and Jin 2022), when inferring s_r using h^s , we use $\min(r, r^t)$, where r^t denotes the maximum scale seen during training. In practice, since all intermediate representations in the hyper-network are suitably structured for convolution, we implement the f_θ employing 1×1 convolution.

Convolution filters ($C_e \cdot k^2$) are predicted batch-wise, and in all cases, k is set to 3.

4.3 Quantitative Results

To validate the importance of multi-scale training and the superiority of our proposed methods, we compare IGConv and IGConv⁺ with SPConv and SPConv⁺ on a variety of encoders (EDSR (Lim et al. 2017), SMFANet (Zheng et al. 2024), HiT-SRF (Zhang, Zhang, and Yu 2024), SRFormer (Zhou et al. 2023), MambaIR (Guo et al. 2024)) with various core operators (convolution, self-attention, and state-space model), datasets (DIV2K, and DF2K (Timofte et al. 2017)), and decoder complexity (SPConv, and SPConv⁺), respectively. For performance evaluation, we leverage five commonly used datasets (Set5 (Bevilacqua et al. 2012), Set14 (Zeyde, Elad, and Protter 2012), B100 (Martin et al. 2001), Urban100 (Huang, Singh, and Ahuja 2015), and Manga109 (Matsui et al. 2017)), and measure Peak Signal to Noise Ratio (PSNR) and Structural Similarity Index Measure (SSIM) in the y-channel after cropping the image’s boundary according to scale. The training details are provided in the Appendix D. In Table 2, and Table 3, IGConv maintains comparable performance to SPConv and SPConv⁺ while reducing training budget and stored parameters by one-third, indicating that scale-specific training is not essential. In addition, SRFormer-IGConv⁺ outperforms SRFormer-SPConv⁺ by 0.25dB at Urban100 $\times 4$, highlighting the superior performance of IGConv⁺ and demonstrating that the additional methods introduced in IGConv⁺ contribute significantly to this performance improvement. Ablation

tion studies for each method can be found in the Appendix E.

Table 4: Comparison on SPConv, SPConv⁺, IGConv and IGConv⁺ on efficiency measures. Metrics are calculated by reconstructing an HD (1280×720) image for each scale using an A6000 GPU.

Upsampler	Latency (ms)			Params (K)			Memory (mb)		
	×2	×3	×4	×2	×3	×4	×2	×3	×4
SPConv	0.41	0.23	0.25	6.9	15.6	27.7	77.4	46.1	38.9
IGConv _{inst}	4.14	3.92	4.90	149.4	334.1	297.2	508.8	475.5	467.2
SPConv ⁺	1.97	1.50	1.47	34.6	77.8	138.2	197.9	166.1	156.0

Furthermore, to demonstrate IGConv’s exceptional efficiency, we compare our methods with SPConv and SPConv⁺ on efficiency measures. As shown in Table 4, IGConv_{inst} exhibits the same computational cost as SPConv while reducing substantial training budget and stored parameters. Notably, IGConv_{inst}⁺ demonstrates less latency, parameters, and memory usage than SPConv⁺ since all computations are computed in LR space, highlighting our method’s remarkable efficiency.

These quantitative comparisons demonstrate that IGConv and IGConv⁺ surpass SPConv and SPConv⁺ in both performance and efficiency, underscoring the importance of multi-scale training.

4.4 Analysis on Inter-Scale Correlations

To illustrate the impact of \mathcal{H} mapping inter-scale correlations (relative position and size) to convolutional filters, we visualise the convolutional filter in RDN-IGConv⁺ at different scales (×2, ×3, ×4, ×32). As shown in Figure 5, the convolution filters at all scales consistently change continuously in response to the variation of r , indicating that \mathcal{H} effectively mapped the inter-scale correlation to the convolution filters.

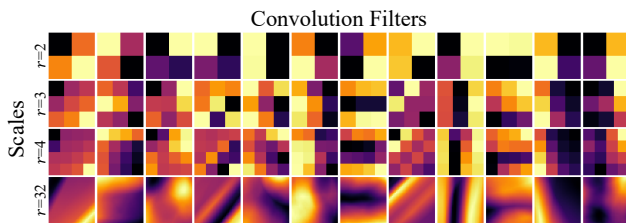


Figure 5: Visualizations of 16 convolution filters in front inferred by \mathcal{H} of RDN-IGConv⁺ for scales ×2, ×3, ×4, and ×32. More visualization is provided in the Appendix F.

4.5 Visual Results

To demonstrate that IGConv and IGConv⁺ are also visually superior, we compare our methods visually to SPConv and then to SPConv⁺. As shown in Figure 6, using IGConv and IGConv⁺ improves the visual quality and the PSNR. This shows that our method yields visually pleasing and numerical results, emphasizing the importance of learning multi-scale again.

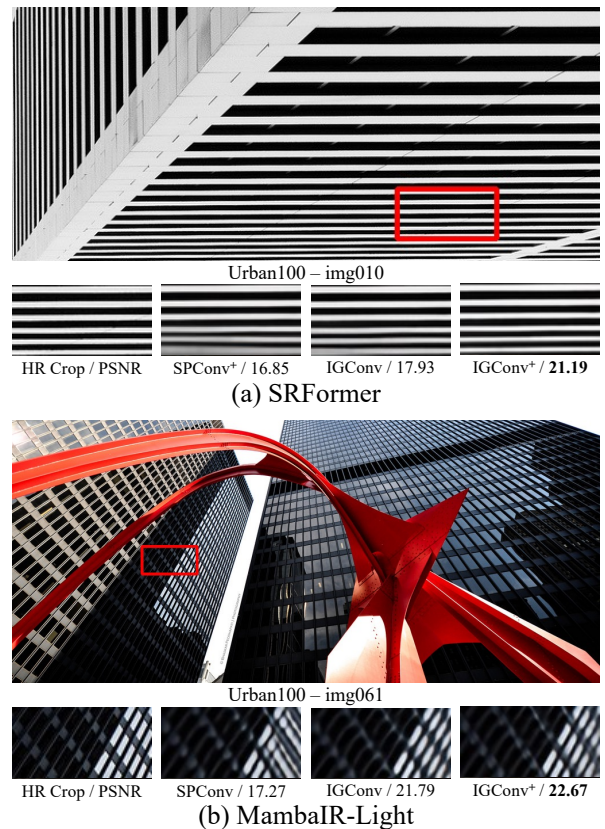


Figure 6: Visual comparisons on SPConv, SPConv⁺, IGConv, and IGConv⁺ on Urban100×4 dataset.

5 Conclusion

This paper addressed the redundancy of classic fixed-scale SR methods, which require a single model for a single fixed-scale by training multiple scales simultaneously. Based on the observation that encoders at different scales generate similar features and that SPConv operates in a highly correlated manner across all scales, we train multiple integer scales with a single model by using a single encoder and introducing IGConv, which integrates SPConv across all scales. We achieved a one-third reduction in both the training budget and the number of stored parameters while maintaining comparable performance to methods trained on a single fixed scale by simultaneously training on multiple integer scales. Additionally, we introduced IGConv⁺, which enhanced performance by employing frequency loss, IGSample, and FGRep. As a result, SRFormer-IGConv⁺ achieved a significant improvement of 0.33 dB in PSNR on the Urban100×2 dataset compared to SRFormer-SPConv⁺, with reduced training budget, stored parameters, and inference cost.

Discussion: Multi-scale training with IGConv⁺ significantly improved performance, but degree of improvement varies. This suggests that a new approach is needed when proposing architectures suitable for multi-scale training and raises the need for further research.

References

- Bevilacqua, M.; Roumy, A.; Guillemot, C.; and Alberi-Morel, M. L. 2012. Low-complexity single-image super-resolution based on nonnegative neighbor embedding.
- Cao, J.; Wang, Q.; Xian, Y.; Li, Y.; Ni, B.; Pi, Z.; Zhang, K.; Zhang, Y.; Timofte, R.; and Van Gool, L. 2023. Ciaosr: Continuous implicit attention-in-attention network for arbitrary-scale image super-resolution. In *Proceedings of the IEEE/CVF Conference on Computer Vision and Pattern Recognition*, 1796–1807.
- Chen, H.-W.; Xu, Y.-S.; Hong, M.-F.; Tsai, Y.-M.; Kuo, H.-K.; and Lee, C.-Y. 2023a. Cascaded local implicit transformer for arbitrary-scale super-resolution. In *Proceedings of the IEEE/CVF Conference on Computer Vision and Pattern Recognition*, 18257–18267.
- Chen, X.; Wang, X.; Zhou, J.; Qiao, Y.; and Dong, C. 2023b. Activating more pixels in image super-resolution transformer. In *Proceedings of the IEEE/CVF conference on computer vision and pattern recognition*, 22367–22377.
- Chen, Y.; Liu, S.; and Wang, X. 2021. Learning continuous image representation with local implicit image function. In *Proceedings of the IEEE/CVF conference on computer vision and pattern recognition*, 8628–8638.
- Dong, C.; Loy, C. C.; He, K.; and Tang, X. 2015. Image super-resolution using deep convolutional networks. *IEEE transactions on pattern analysis and machine intelligence*, 38(2): 295–307.
- Guo, H.; Li, J.; Dai, T.; Ouyang, Z.; Ren, X.; and Xia, S.-T. 2024. Mambair: A simple baseline for image restoration with state-space model. *arXiv preprint arXiv:2402.15648*.
- He, Z.; and Jin, Z. 2024. Latent Modulated Function for Computational Optimal Continuous Image Representation. In *Proceedings of the IEEE/CVF Conference on Computer Vision and Pattern Recognition*, 26026–26035.
- Hu, X.; Mu, H.; Zhang, X.; Wang, Z.; Tan, T.; and Sun, J. 2019. Meta-SR: A magnification-arbitrary network for super-resolution. In *Proceedings of the IEEE/CVF conference on computer vision and pattern recognition*, 1575–1584.
- Huang, J.-B.; Singh, A.; and Ahuja, N. 2015. Single image super-resolution from transformed self-exemplars. In *Proceedings of the IEEE conference on computer vision and pattern recognition*, 5197–5206.
- Lai, W.-S.; Huang, J.-B.; Ahuja, N.; and Yang, M.-H. 2017. Deep laplacian pyramid networks for fast and accurate super-resolution. In *Proceedings of the IEEE conference on computer vision and pattern recognition*, 624–632.
- Lee, J.; and Jin, K. H. 2022. Local texture estimator for implicit representation function. In *Proceedings of the IEEE/CVF conference on computer vision and pattern recognition*, 1929–1938.
- Li, A.; Zhang, L.; Liu, Y.; and Zhu, C. 2023. Feature modulation transformer: Cross-refinement of global representation via high-frequency prior for image super-resolution. In *Proceedings of the IEEE/CVF International Conference on Computer Vision*, 12514–12524.
- Liang, J.; Cao, J.; Sun, G.; Zhang, K.; Van Gool, L.; and Timofte, R. 2021. Swinir: Image restoration using swin transformer. In *Proceedings of the IEEE/CVF international conference on computer vision*, 1833–1844.
- Lim, B.; Son, S.; Kim, H.; Nah, S.; and Mu Lee, K. 2017. Enhanced deep residual networks for single image super-resolution. In *Proceedings of the IEEE conference on computer vision and pattern recognition workshops*, 136–144.
- Liu, W.; Lu, H.; Fu, H.; and Cao, Z. 2023a. Learning to upsample by learning to sample. In *Proceedings of the IEEE/CVF International Conference on Computer Vision*, 6027–6037.
- Liu, Y.; Dong, H.; Liang, B.; Liu, S.; Dong, Q.; Chen, K.; Chen, F.; Fu, L.; and Wang, F. 2023b. Unfolding once is enough: A deployment-friendly transformer unit for super-resolution. In *Proceedings of the 31st ACM International Conference on Multimedia*, 7952–7960.
- Martin, D.; Fowlkes, C.; Tal, D.; and Malik, J. 2001. A database of human segmented natural images and its application to evaluating segmentation algorithms and measuring ecological statistics. In *Proceedings Eighth IEEE International Conference on Computer Vision. ICCV 2001*, volume 2, 416–423. IEEE.
- Matsui, Y.; Ito, K.; Aramaki, Y.; Fujimoto, A.; Ogawa, T.; Yamasaki, T.; and Aizawa, K. 2017. Sketch-based manga retrieval using manga109 dataset. *Multimedia tools and applications*, 76: 21811–21838.
- Ray, A.; Kumar, G.; and Kolekar, M. H. 2024. CFAT: Unleashing Triangular Windows for Image Super-resolution. In *Proceedings of the IEEE/CVF Conference on Computer Vision and Pattern Recognition*, 26120–26129.
- Shi, W.; Caballero, J.; Huszár, F.; Totz, J.; Aitken, A. P.; Bishop, R.; Rueckert, D.; and Wang, Z. 2016. Real-time single image and video super-resolution using an efficient sub-pixel convolutional neural network. In *Proceedings of the IEEE conference on computer vision and pattern recognition*, 1874–1883.
- Song, G.; Sun, Q.; Zhang, L.; Su, R.; Shi, J.; and He, Y. 2023. OPE-SR: Orthogonal position encoding for designing a parameter-free upsampling module in arbitrary-scale image super-resolution. In *Proceedings of the IEEE/CVF Conference on Computer Vision and Pattern Recognition*, 10009–10020.
- Sun, L.; Pan, J.; and Tang, J. 2022. Shufflemixer: An efficient convnet for image super-resolution. *Advances in Neural Information Processing Systems*, 35: 17314–17326.
- Timofte, R.; Agustsson, E.; Van Gool, L.; Yang, M.-H.; and Zhang, L. 2017. Ntire 2017 challenge on single image super-resolution: Methods and results. In *Proceedings of the IEEE conference on computer vision and pattern recognition workshops*, 114–125.
- Tu, Z.; Talebi, H.; Zhang, H.; Yang, F.; Milanfar, P.; Bovik, A.; and Li, Y. 2022. Maxim: Multi-axis mlp for image processing. In *Proceedings of the IEEE/CVF conference on computer vision and pattern recognition*, 5769–5780.
- Vasconcelos, C. N.; Oztireli, C.; Matthews, M.; Hashemi, M.; Swersky, K.; and Tagliasacchi, A. 2023. Cuf: Continuous upsampling filters. In *Proceedings of the IEEE/CVF Conference on Computer Vision and Pattern Recognition*, 9999–10008.
- Vaswani, A.; Shazeer, N.; Parmar, N.; Uszkoreit, J.; Jones, L.; Gomez, A. N.; Kaiser, Ł.; and Polosukhin, I. 2017. Attention is all you need. *Advances in neural information processing systems*, 30.
- Wang, X.; Chen, X.; Ni, B.; Wang, H.; Tong, Z.; and Liu, Y. 2023. Deep arbitrary-scale image super-resolution

via scale-equivariance pursuit. In *Proceedings of the IEEE/CVF Conference on Computer Vision and Pattern Recognition*, 1786–1795.

Wang, Z.; Wu, S.; Xie, W.; Chen, M.; and Prisacariu, V. A. 2021. NeRF-: Neural radiance fields without known camera parameters. *arXiv preprint arXiv:2102.07064*.

Zamir, S. W.; Arora, A.; Khan, S.; Hayat, M.; Khan, F. S.; and Yang, M.-H. 2022. Restormer: Efficient transformer for high-resolution image restoration. In *Proceedings of the IEEE/CVF conference on computer vision and pattern recognition*, 5728–5739.

Zeyde, R.; Elad, M.; and Protter, M. 2012. On single image scale-up using sparse-representations. In *Curves and Surfaces: 7th International Conference, Avignon, France, June 24-30, 2010, Revised Selected Papers 7*, 711–730. Springer.

Zhang, L.; Li, Y.; Zhou, X.; Zhao, X.; and Gu, S. 2024. Transcending the limit of local window: Advanced super-resolution transformer with adaptive token dictionary. In *Proceedings of the IEEE/CVF Conference on Computer Vision and Pattern Recognition*, 2856–2865.

Zhang, X.; Zeng, H.; Guo, S.; and Zhang, L. 2022. Efficient long-range attention network for image super-resolution. In *European conference on computer vision*, 649–667. Springer.

Zhang, X.; Zhang, Y.; and Yu, F. 2024. HiT-SR: Hierarchical Transformer for Efficient Image Super-Resolution. *arXiv preprint arXiv:2407.05878*.

Zhang, Y.; Li, K.; Li, K.; Wang, L.; Zhong, B.; and Fu, Y. 2018a. Image super-resolution using very deep residual channel attention networks. In *Proceedings of the European conference on computer vision (ECCV)*, 286–301.

Zhang, Y.; Tian, Y.; Kong, Y.; Zhong, B.; and Fu, Y. 2018b. Residual dense network for image super-resolution. In *Proceedings of the IEEE conference on computer vision and pattern recognition*, 2472–2481.

Zheng, M.; Sun, L.; Dong, J.; and Pan, J. 2024. SMFANet: A Lightweight Self-Modulation Feature Aggregation Network for Efficient Image Super-Resolution. In *ECCV*.

Zhou, Y.; Li, Z.; Guo, C.-L.; Bai, S.; Cheng, M.-M.; and Hou, Q. 2023. Srformer: Permuted self-attention for single image super-resolution. In *Proceedings of the IEEE/CVF International Conference on Computer Vision*, 12780–12791.

The Appendix includes detailed comparisons with similar methods, experiments beyond the $\times 4$ scale, training details, an ablation study, additional visualizations of inter-scale correlation, and quantitative and qualitative results on ASSR methods.

A Comparisons on LapSRN and MDSR

Before our research, attempts were made to train multiple scales simultaneously. For example, LapSRN aimed to stably predict $\times 8$ images by progressively upsampling the LR image. MDSR extracts features from an image and converts them to RGB using scale-specific heads and tails, while sharing a feature extractor across all scales to extract features from multiple scales. Our approach offers several advantages over these methods. First, LapSRN requires computations in the high-resolution (HR) space because of its progressive upsampling, resulting in a significant computational burden. We demonstrate in Appendix C that our method can predict the $\times 8$ scale without such excessive computational costs. Additionally, MDSR independently trains each head and tail, which means the heads and tails cannot learn multi-scale information, potentially negatively impacting performance.

B Comparisons on CUF

The continuous upsampling filter (CUF) (Vasconcelos et al. 2023) is similar to our method of mapping kernels to INR and converting efficiently when instantiated at a particular scale. However, our method is more computationally efficient. To demonstrate the computational efficiency of our approach compared to CUF, we consider only the instantiated CUF at specific scales, excluding the inefficiencies that arise from targeting Arbitrary-Scale Super-Resolution (ASSR). CUF performs scale-variant modulation using depth-wise convolution followed by depth-to-space (\mathcal{DS}) to upsample, with two additional 1×1 convolutions added to compensate for insufficient channel mixing. These additional convolutions result in computational inefficiency, involving extra computations in the upsampled HR space, similar to SPConv⁺. In Appendix G, we demonstrate that Instantiated IGConv⁺ outperforms Instantiated CUF in both latency and performance, highlighting the superiority of our approach that performing all heavy computation in Low-Resolution (LR) space.

C Beyond $\times 4$ scale

Many recent SR studies have focused on three scales ($\times 2$, $\times 3$, and $\times 4$), and accordingly, we also trained and evaluated our model on these three scales. However, some previous studies have evaluated four scales, including $\times 8$, which raised the question of whether more challenging and complex scales can also be trained simultaneously. For this reason, we used RCAN (Zhang et al. 2018a) as the encoder to train and evaluate our model on four scales simultaneously, including $\times 8$. As shown in Table 7, IGConv⁺ achieves a PSNR that is 0.13 dB higher on Urban100 $\times 8$ compared to SPConv⁺, even though IGConv⁺ was trained on four scales simultaneously. This surprising result underscores our

claim that a fixed-scale training approach is unnecessary and shows that learning high scales is possible without a progressive upsampling architecture.

D Training Details

This section describes training details to train each method. The training details presented in Table 5 correspond to the training budget used by each method to the $\times 2$ scale.

Table 5: Training Details for each method.

Methods	PatchSize	BatchSize	Iteration	LR	EMA
EDSR	48	16	300000	0.0001	✓
RCAN	48	16	1000000	0.0001	✗
SMFANet	64	64	1000000	0.001	✓
HiT-SRF	64	64	500000	0.0005	✗
SRFormer	64	32	500000	0.0002	✗
MambaIR-light	64	32	500000	0.0002	✗
MambaIR	64	32	500000	0.0002	✗

E Ablation Study

To validate that every proposed method contributes to performance improvement, we perform an ablation study by adding our proposal to RDN (Zhang et al. 2018b). Table 6 demonstrates the performance improvement by replacing the upsampler with IGConv and adding frequency loss, IGSample, and FGRep. This indicates that our proposed methods effectively contribute to performance improvement.

Table 6: Ablation study on our proposed methods. FFT, IGS, and FGR denote frequency loss, IGSample, and FGRep, respectively.

Upsampler	FFT	IGS	FGR	Urban100		
				$\times 2$	$\times 3$	$\times 4$
SPConv ⁺	✗	✗	✗	32.89	28.80	26.61
IGConv	✗	✗	✗	33.06	28.97	26.82
IGConv ⁺	✓	✗	✗	33.10	29.02	26.88
	✓	✓	✗	33.15	29.08	26.95
	✓	✓	✓	33.17	29.12	26.96

F More Visualizations on Inter-Scale Corr.

This section includes additional visualizations of inter-scale correlations. As shown in Figure 7, all convolution filters change continuously with variations in scale, demonstrating that \mathcal{H} effectively captures the inter-scale correlation.

G Comparison on ASSR

We compare our method to ASSR methods, as training more than one scale with a single model shares similarities with these methods. For the comparison, we train and evaluate our upsampler, IGConv⁺, using RDN (Zhang et al. 2018b) and SwinIR (Liang et al. 2021), which are commonly used as encoders in ASSR methods. The baselines for comparison include LIIF (Chen, Liu, and Wang 2021),

Table 7: comparisons of fixed-scale upsamplers (SPConv, SPConv+) and our proposed multi-scale upsamplers (IGConv, IGConv+) on RCAN encoder.

Encoder	Scale	Decoder	Set5	Set14	B100	Urban100	Manga109
RCAN	2	SPConv ⁺	38.27/0.9614	34.12/0.9216	32.41/0.9027	33.34/0.9384	39.44/0.9786
		IGConv ⁺	38.23/0.9614	34.12/0.9217	32.38/0.9022	33.27/0.9383	39.39/0.9784
	3	SPConv ⁺	34.74/0.9299	30.65/0.8482	29.32/0.8111	29.09/0.8702	34.44/0.9499
		IGConv ⁺	34.86/0.9306	30.71/0.8490	29.34/0.8111	29.18/0.8712	34.66/0.9505
	4	SPConv ⁺	32.63/0.9002	28.87/0.7889	27.77/0.7436	26.82/0.8087	31.22/0.9173
		IGConv ⁺	32.68/0.9007	28.98/0.7907	27.83/0.7444	27.03/0.8118	31.60/0.9182
	8	SPConv ⁺	27.31/0.7878	25.23/0.6511	24.98/0.6058	23.00/0.6452	25.24/0.8029
		IGConv ⁺	27.34/0.7850	25.35/0.6513	25.04/0.6048	23.13/0.6454	25.45/0.8016

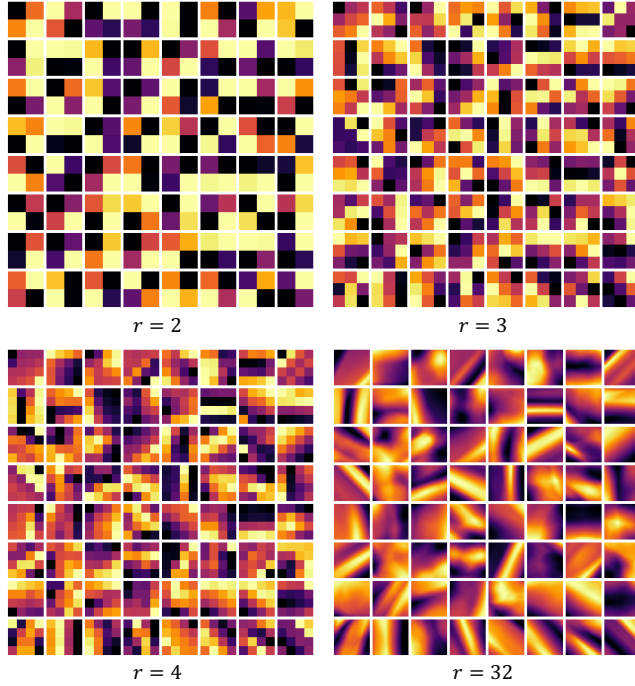


Figure 7: Visualizations of convolution filters inferred by \mathcal{H} of RDN-IGConv⁺ for scales $\times 2$, $\times 3$, $\times 4$, and $\times 32$.

LTE (Lee and Jin 2022), CiaoSR (Cao et al. 2023), OPE-SR (Song et al. 2023), CUF (Vasconcelos et al. 2023), and LM-LTE (He and Jin 2024). As shown in Table 9, SwinIR-IGConv⁺ achieves a 0.01 dB higher PSNR on B100 $\times 4$ compared to SwinIR-CiaoSR while reducing latency and memory usage by 99.5% and 99.4%, respectively, demonstrating exceptional performance-efficiency trade-off. Moreover, IGConv⁺_{inst} outperforms the CUF instantiated at a specific integer scale by achieving a 0.06 dB higher PSNR on Urban100 $\times 2$, with 78% and 86% lower latency and memory usage, respectively, showing that our efficiency is not merely due to the absence of non-integer scale prediction.

We also visually compare IGConv⁺ with the ASSR methods (LIIF, LTE, and OPE-SR). In Figure 8, IGConv⁺ has good visual quality and PSNR compared to the ASSR method, which requires a substantial computational cost.

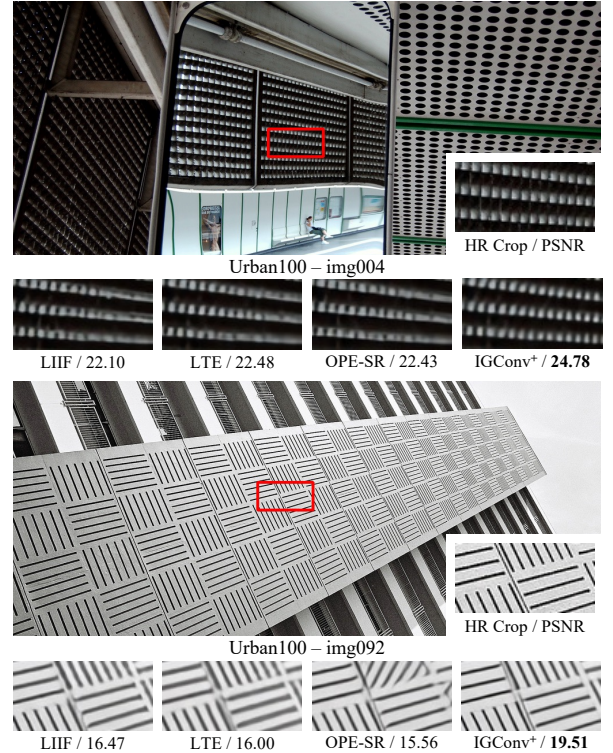


Figure 8: Visual comparisons on IGConv⁺ and ASSR methods using RDN encoder on Urban100 $\times 4$ dataset.

This confirms that IGConv⁺ is efficient and has superior visual quality to the ASSR methods, highlighting the exceptional performance-efficiency trade-off of our method.

H IGConv for ASSR

Since our method’s core operator is convolution, it cannot upsample to an arbitrary scale. However, predicting $[r \in \mathbb{R}]$ and then downsampling to r could approximate the desired result, although this approach is not optimal. We train and evaluate IGConv⁺_{arb}, which learns scales in the range $r \in [1, 4]$ using the aforementioned method to predict arbitrary-scale and compare it with ASSR methods on non-integer scales. As shown in Table 9, despite its naive

Table 8: Comparison of ASSR upsamplers with our proposal. Efficiency measures are calculated by upsampling a 128x128 image using an A6000 GPU for $\times 4$ scale. The best and second-best results are highlighted in bold and underlined, respectively.

Encoder	Decoder	Latency (ms)	#Params (K)	Memory (mb)	Set5			Set14			B100			Urban100		
					$\times 2$	$\times 3$	$\times 4$	$\times 2$	$\times 3$	$\times 4$	$\times 2$	$\times 3$	$\times 4$	$\times 2$	$\times 3$	$\times 4$
RDN	LIIF	139.6	347	1811	38.17	34.68	32.50	33.97	30.53	28.80	32.32	29.26	27.74	32.87	28.82	26.68
	LTE	166.0	494	1608	38.23	34.72	32.61	34.09	30.58	28.88	32.36	29.30	27.77	33.04	28.97	26.81
	CiaoSR	395.5	1429	12378	38.29	34.85	32.66	34.22	30.65	28.93	32.41	29.34	27.83	33.30	29.17	27.11
	LM-LTE	31.2	271	367	38.23	<u>34.76</u>	32.53	<u>34.11</u>	30.56	28.86	32.37	29.31	27.78	33.03	28.96	26.80
	OPE-SR	15.6	0	339	37.60	34.59	32.47	33.39	30.49	28.80	32.05	29.19	27.72	31.78	28.63	26.53
	CUF	- / 1.2 [§]	10	- / 132 [§]	38.23	34.72	32.54	33.99	30.58	28.86	32.35	29.29	27.76	33.01	28.91	26.75
	IGConv⁺	2.3 / 0.5[§]	922	71 / 43[§]	<u>38.26</u>	<u>34.74</u>	<u>32.64</u>	34.10	30.68	28.91	<u>32.39</u>	<u>29.33</u>	<u>27.82</u>	<u>33.17</u>	<u>29.11</u>	<u>26.96</u>
SwinIR	LIIF	342.8	614	5015	38.28	34.87	32.73	34.14	30.75	28.98	32.39	29.34	27.84	33.36	29.33	27.15
	LTE	166.0	1028	1619	38.33	<u>34.89</u>	<u>32.81</u>	34.25	30.80	29.06	32.44	29.39	27.86	33.50	29.41	27.24
	CiaoSR	889.9	3168	34760	38.38	34.91	32.84	34.33	30.82	<u>29.08</u>	32.47	29.42	<u>27.90</u>	33.65	<u>29.52</u>	27.42
	LM-LTE	31.4	538	376	38.32	34.88	32.77	34.28	30.79	29.01	<u>32.46</u>	29.39	27.87	33.52	29.44	27.24
	CUF	- / 3.6 [§]	37	- / 376 [§]	38.34	34.88	32.80	<u>34.29</u>	30.79	29.02	32.45	29.38	27.85	33.54	29.45	27.24
	IGConv⁺	4.6 / 0.8[§]	1991	215 / 52[§]	<u>38.35</u>	<u>34.89</u>	<u>32.79</u>	34.18	30.84	29.09	<u>32.46</u>	<u>29.41</u>	27.91	<u>33.60</u>	29.53	<u>27.35</u>

Table 9: Comparison of ASSR upsamplers with our proposal on non-integer scales. The best and second-best results are highlighted in bold and underlined, respectively.

Encoder	Decoder	Set5			Set14			B100			Urban100		
		$\times 1.5$	$\times 2.5$	$\times 3.5$	$\times 1.5$	$\times 2.5$	$\times 3.5$	$\times 1.5$	$\times 2.5$	$\times 3.5$	$\times 1.5$	$\times 2.5$	$\times 3.5$
RDN	LIIF	41.43	36.15	33.56	37.45	31.87	29.56	35.83	30.48	28.42	<u>36.79</u>	30.49	27.64
	LTE	41.51	36.18	33.64	37.55	31.91	<u>29.62</u>	<u>35.87</u>	<u>30.51</u>	28.45	36.97	30.64	<u>27.77</u>
	LM-LTE	<u>41.49</u>	<u>36.18</u>	<u>33.62</u>	<u>37.52</u>	<u>31.91</u>	29.58	35.88	30.52	<u>28.45</u>	36.97	30.62	<u>27.77</u>
	OPE-SR	40.24	35.85	33.49	36.02	31.67	29.55	35.07	30.33	28.38	33.47	30.08	27.48
	IGConv⁺_{arb}	41.25	36.20	33.64	37.40	32.00	29.68	35.74	<u>30.51</u>	28.46	36.64	30.70	27.85

implementation, IGConv⁺_{arb} achieves results comparable to other methods.